Preparation of Hybrid Films Based in Aluminum 8-hydroxyquinoline for Application in Organic Light-emitting Devices

María Elena Sánchez Vergara * , Luis Alberto Cantera Cantera , Citlalli Ríos , Roberto Salcedo

Posted Date: 13 July 2023

doi: 10.20944/preprints202307.0905.v1

Keywords: Hydroxyquinoline; DFT Calculations; Hybrid Film; Optical Properties; Organic Light-emitting Device

Article

Preparation of Hybrid Films Based in Aluminum 8-Hydroxyquinoline for Application in Organic Light-Emitting Devices

María Elena Sánchez Vergara [1,*], Luis Alberto Cantera Cantera [1], Citlalli Ríos [2] and Roberto Salcedo [2]

[1] Facultad de Ingeniería, Universidad Anáhuac México, Avenida Universidad Anáhuac 46, Col. Lomas Anáhuac, Huixquilucan 52786, Estado de México, México; elena.sanchez@anahuac.mx (M.E.S.V.); calberto@anahuac.mx (L.A.C.C.)

[2] Instituto de Investigaciones en Materiales, Universidad Nacional Autónoma de México, Circuito Exterior s/n. C.U., Delegación Coyoacán, C.P. 04510. Ciudad de México, México; citriogo@yahoo.com.mx (C.R.); salcevitch@gmail.com (R.S.)

* Correspondence: elena.sanchez@anahuac.mx (M.E.S.V.)

Abstract: In the present work we have investigated an organic semiconductor based on tris(8-hydroxyquinoline) aluminum (AlQ_3) doped with tetracyanoquinodimethane (TCNQ), which can be used as a photoactive layer in organic light-emitting device (OLED). DFT calculations were carried out to optimize the structure of semiconductor species and get related constants in order to compare experimental and theoretical results. The semiconductor AlQ_3-TCNQ was structurally characterized and their experimental IR spectrum was compared with that obtained through DFT calculations. Subsequently, AlQ_3-TCNQ films with polypyrrole (PPy) matrix were fabricated, they were morphologically and mechanically characterized by Scanning Electron and Atomic Force Microscopy techniques. The maximum stress for the film is 8.66 MPa and the Knoop hardness is 0.0311. The film was analyzed in its optical behavior and the optical properties of hybrid film were found to exhibit two indirect allowed transitions at 2.64 and 3.44 eV. Finally, an OLED type was fabricated that was electrically characterized. Applying a cubic-spline approximation to fit cubic polynomials to the J-V curves, the ohmic to SCLC transition voltage V_{ON} and the trap-filled-limit voltage V_{TFL} for the device were obtained. Then, the free carrier density and trap density for the device were approximated to $n_0 = 2.4787 \times 10^{17} \frac{1}{m^3}$ and $N_t = 1.7419 \times 10^{29} \frac{1}{m^3}$ respectively.

Keywords: hydroxyquinoline; DFT calculations; hybrid film; optical properties; organic light-emitting device

1. Introduction

The development of optoelectronic and photovoltaic devices based on organic semiconductors has drawn attention because of their promising applications [1–3]. Organic semiconductors require a conjugated structure to be able to participate effectively in charge transport [1,2]. The surface of their π orbitals should allow the stabilization of the electronic charge by resonant effect, and also to facilitate intermolecular interactions by overlapping orbitals. It is for this reason that the correct selection of the organic base structure is a determining aspect in the design of new organic semiconductors. Within the different types of organic semiconductors, the small π-conjugated molecules have grabbed the attention due to their attractive features such as well-defined chemical structure, easy modified structural layouts, fine-tuning of their energy levels, and excellent reproducibility [4–8]. Small π-conjugated molecules can be processed in solution [7], besides there is the fact that due to their low molecular weight [4,9], they can also be deposited by vacuum thermal evaporation for ordered layers that improve the performance of the final device. Vacuum thermal deposition produces devices that have controlled multilayers and stability suitable for their

commercialization. However, it is required to have small π-conjugated molecules with sufficiently high thermal stability and better light harvesting capability [9]. It is for this reason that solution deposition methods are also used in the processing of small molecules in solution or dispersion [10–13]. This latter feature gives several advantages, such as the possibility of preparing thin films with insoluble molecules with high chemical stability, which, when forming part of photovoltaic and optoelectronic devices, will enhance their service conditions without degrading easily.

Metal-Quinolines (MQ) are small molecules that has been used in organic optoelectronic devices [14–18] due to its ability to form thin films in solution [19–22] and by evaporation [15,18,23,24], since it presents high chemical and thermal stability. It also presents easy color tunability with simple synthesis [25–28], magnetism properties [29] and electron transport behavior [19,25,30]. Besides, the fluorescence of MQs has resulted in its classification as an important class of electro-luminiscent/electron transport materials [19]. Changing the central metal ion affects the luminescence peak position of the MQ [14,16–19,31]. Within the MQs family, the tris(8-hydroxyquinoline) aluminum (Alq_3) is the most popular MQ's semiconductor due to its strong luminesce, high electron mobility, and in addition, due to its low cost and simple technology of fabrication [23,32]. Alq_3 is a small molecule with conjugated π-electron systems and has a non-centrosymmetric crystal structure [32] with ∝, β, γ, δ and ε crystalline phases [32–36]. Alq_3 has become used to fabricate thin films by solution process or by using vacuum thermal deposition [23,36] therefore, a considerable number of studies are concentrated on the nucleation and growth of Alq_3 films [37] as well as on their surface topography [38], their optical properties and their energy band gap under indirect and direct conditions [23]. In addition to that above pointed, it should be considered that many studies have investigated the applications of Alq_3 films on organic light-emitting devices (OLEDs) [20,32,39], display devices and systems [40], and organic photovoltaic cells [41]. However, few studies have been devoted to understand the current-voltage characteristics in order to manipulate doping and improve the performance of Alq_3, focusing mainly on the electrical conduction mechanism analysis such as transition from the ohmic to space-charge limited current (SCLC) regimes [42,43], as well as in the estimation of electrical parameters such as trap factors, free carrier density, ohmic to SCLC transition voltage, trap-filled-limit voltage [44–46].

Although space-charge limited current theory dates to the 1940s through the work of Mott and Gurney [47], the study of ohmic and space-charge limited currents in semiconductors is the most widely used to explain the mechanisms of charge transport and carrier trapping. In the case of the SCLC regime, it is presented when the electrode injects more carriers than the material can transport and is modeled by a quadratic equation. On the other hand, the ohmic regime has a linear behavior and is presented when the amount of injected is low compared to thermally generated carriers and impurities [42,43].

The aim of the present work is to employ Alq_3 as a small molecule to produce active layers of an OLED type device with one-layer structure formed by Alq_3 doped with tetracyanoquinodimethane (Alq_3-TCNQ). The TCNQ is an electronic-acceptor capable of forming stable radicals, with valence electrons located above and below the median plane of the molecule, in delocalized π orbitals [48,49]. The TCNQ favors the formation of molecular anisotropic blocks, where conduction channels are generated. Subsequently, the Alq_3-TCNQ doped semiconductor was embedded in a polypyrrole (PPy) polymeric matrix, in order to fabricate a hybrid active layer, with dispersed heterojunction architecture. In this layer there is a high contact surface between Alq_3 and TCNQ, which favors the diffusion of excitons. Furthermore, the PPy choice is due to its conductive properties and moderate band gap, caused by its heteroatoms and π-conjugated system [50]. The PPy present a unique combination of environmental stability, and structural versatility which allows it to be used as a matrix in the fabrication of heterojunction hybrid films. The (Alq_3-TCNQ):PPy film was structurally and morphologically characterized to later be evaluated for its optical properties. Finally, an OLED was fabricated with the hybrid film, and the electrical characteristics were investigated by current-voltage measurements and the conduction mechanisms in the OLED type device can be explained by theoretical model. Also, based on the current-voltage measurements of the device and its approximation by cubic-splines, the ohmic to SCLC transition voltage V_{ON} and the trap-filled-limit

Preprints (www.preprints.org) | NOT PEER-REVIEWED | Posted: 13 July 2023 doi:10.20944/preprints202307.0905.v1

voltage V_{TFL} were obtained. With respect of the theoretical calculations, a DFT method was used to optimize the structure of Alq_3-TCNQ semiconductor complexes, their IR spectra were calculated and compared to those experimentally obtained. Additionally, their frontier molecular orbitals were obtained and with these results the corresponding bandgap values were calculated.

2. Theoretical Calculations

The structural characterization of the parent molecules Alq_3 and TCNQ as well as the Alq_3-TCNQ semiconductor was carried out by using B3PW91 hybrid method contained in Gaussian 16 Package [51] and the 6-31G basis set. The method is based on the combination of Becke's gradient corrections [52] for exchange and Perdew–Wang's for correlation [53]. Frequency calculations were carried out at the same level of theory in order to confirm that the optimised structures were at the minimum of the potential energy surface.

3. Materials and Methods

Tris-(8-hydroxyquinoline)aluminum (Alq_3; $C_{27}H_{18}AlN_3O_3$), 7,7,8,8-tetracyanoquinodimethane (TCNQ; $C_{12}H_4N_4$) and polypyrrole (PPy) were obtained from Sigma Aldrich (Sigma-Aldrich, St. Louis, MO, USA) and required no further purification. Afterwards an Alq_3-TCNQ doped semiconductor was obtained by dissolution of 106 mg (0.3mmol) of Alq_3 and 102 mg (0.5mmol) of TCNQ in 20 ml of ethanol. Doping was carried out during 30 minutes at 425 K in heated reactor Monowave 50 (Anton Paar México, S.A. de C.V. Hidalgo, México) with pressure sensor. The reactor is operated with a borosilicate glass vial and manually closed by a cover with an integrated pressure (0-20 bar) and temperature sensor. The system was cooled and brought to atmospheric pressure, the Alq_3-TCNQ was filtered, washed whit ethanol and dried in vacuum. The Alq_3-TCNQ semiconductor was subsequently deposited on PPy to form a composite film onto different substrates: glass, high-resistivity monocrystalline n-type silicon wafers (c-Si), and coated glass slides with Fluorine-Tin-Oxide (FTO). The glass, and FTO substrates were previously cut and washed consecutively in an ultrasonic bath with solvents: chloroform, ethanol, and acetone. The silicon substrates, however, were cut and later washed with "p" solution (10 mL HF, 15 mL HNO_3, and 300 mL H_2O). For the manufacture of the film, a 10% dispersion of Alq_3-TCNQ was prepared in PPy previously dissolved in cresol. The mixture Alq_3-TCNQ with PPy was dispersed using the G560 shaker of Scientific Industries Vortex-Genie (Bohemia, NY, USA). To obtain the films a syringe was used to apply 0.6 mL on the substrate surface and then spread the dispersion. Subsequently, the films were brought to 55°C for 5 minutes in the drying oven Briteg SC-92898 (Instrumentos Científicos, S.A de C.V.). This accelerated the film fabrication process and prevented the samples from swelling and cracking during drying. Morphological and topographical characteristics were investigated with a ZEISS EVO LS 10 scanning electron microscope (SEM, Carl Zeiss AG. Jena, Germany) and with a Nano AFM atomic force microscope (AFM, Nanosurf AG, Liesta, Switzerland) using an Ntegra platform for the (Alq_3-TCNQ):PPy films deposited on glass and silicon substrates respectively. To verify the main functional groups of the Alq_3-TCNQ semiconductor, a FTIR spectroscopy analysis was performed, using a Nicolet iS5-FT spectrometer (Thermo Fisher Scientific Inc., Waltham, MA, USA). The UV-vis in films on glass were obtained in the 200-1100 nm wavelength range, on a UV-Vis 300 Unicam spectrophotometer (Thermo Fisher Scientific Inc., Waltham, MA, USA). Finally, the electrical behavior was procured through current-voltage (I-V) measurements in a Keithley 4200-SCS-PK1 auto-ranging pico-ammeter (Tektronix Inc., Beaverton, OR, USA). The evaluation was performed on the FTO/(Alq_3-TCNQ):PPy/Ag device (Figure 1a), Ag was deposited on top of the layers to act as cathode and the FTO act as anode. I-V curves were obtained under darkness, white, red, orange, yellow, green, blue, and ultraviolet lights in a range of -1.2 to 1.2 V at room temperature. The principal studies of the current-voltage (I-V) characteristics in semiconductors are the ohmic and space-charge-limited currents (SCLC), therefore several investigations as [42,43,54–56] have identified a typical current density-voltage curve as is showed in Figure 1b.

Preprints (www.preprints.org) | NOT PEER-REVIEWED | Posted: 13 July 2023 doi:10.20944/preprints202307.0905.v1

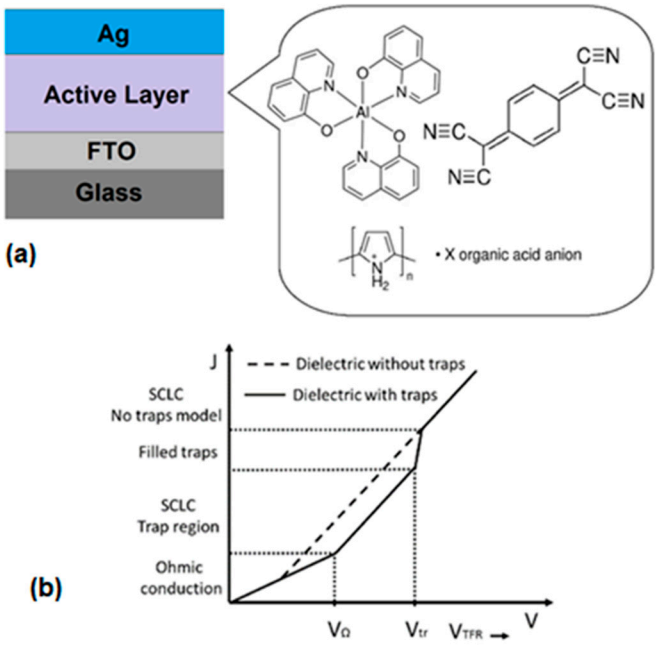

Figure 1. (a) Diagram of the diode type device for electrical characterization. (b) Current density-voltage characteristic [56].

From Figure 1b, two regimes can be identified, the first one is the ohmic regime at low voltages which can be expressed by

$$J_{\Omega} = qn_0\mu_n\frac{V}{d_s}, \tag{1}$$

when the voltage is increased, the second regime is quadratic called space-charge limited current (SCLC) regime defined by

$$J_{\mathrm{SCLC}} = \frac{9}{8}\mu_n\varepsilon_0\varepsilon_r\frac{V^2}{d_s^3}, \tag{2}$$

where J denote the current density, q is the electronic charge, n_0 is the free carrier density, μ_n is the electron mobility, V is the applied voltage, d_s is the thickness of the sample, ε_0 is the vacuum permittivity and ε_r is the dielectric constant. Generally, at high voltages, a SCLC regime also occurs, but with a higher growth rate than the quadratic regime. In addition to the ohmic and SCLC regimes, it has been identified the ohmic to SCLC transition voltage denoted by V_{ON} and the trap-filled-limit voltage denoted by V_{TFL} which determines the change from the quadratic regime to another. These transition voltages are defined by

$$V_{ON} = \frac{8}{9}\frac{qn_0}{\varepsilon_0\varepsilon_r}d_s^2, \tag{3}$$

$$V_{\mathrm{TFL}} = \frac{qN_t}{2\varepsilon_r}d_s^2, \tag{4}$$

where N_t is the trap density. Notice that if the transition voltages are determined, from equations (3) and (4), the free carrier density and the trap density can be calculated.

4. Results and Discussion

4.1. DFT Calculations

To determine the feasibility of the doping the electronic-donor Alq_3 with the electronic-acceptor TCNQ, the molecular geometry of both precursor compounds and the organic semiconductor was optimized by using the DFT method. The energy values of the molecular orbitals HOMO (highest occupied molecular orbital) and LUMO (lowest unoccupied molecular orbital) for hydroxyquinoline

Preprints (www.preprints.org) | NOT PEER-REVIEWED | Posted: 13 July 2023 doi:10.20944/preprints202307.0905.v1

Alq_3, are -5.1 and -1.95 eV respectively, and the band gap value is 3.15 eV. These results are in the same order of magnitude as those calculated by Sevgili et al. [20] for aluminum 8-hydroxyquinoline microbelts and microdots. For the TCNQ, the calculated HOMO value is -7.45 eV, the LUMO has a value of -4.95 eV and the bandgap is 2.5 eV. It should be considered that the band gaps obtained for both precursor species are large to be considered efficient organic semiconductors. The control of the HOMO-LUMO energy gap of organic semiconductors it is fundamental for the effective transport of charges. Hence the importance of calculating interactions between Alq_3 and TCNQ, which can generate a decrease in the energy gap and allow the Alq_3-TCNQ species to perform as an adequate organic semiconductor. To understand the interaction between hydroxyquinoline and TCNQ two possibilities were studied. The first one considering the interaction between central oxygens of hydroxyquinoline and the aromatic ring of TCNQ (HAl-TCNQ1). In a second case the interaction between the hydrogen atoms of one of the rings of hydroxyquinoline and the nitrogen atoms of TCNQ (HAl-TCNQ2) was studied. These two interactions are the unique stable possibilities of dispersion forces interactions and are hydrogen bonds. Figure 2 shows the optimized structures of the mentioned cases in which the mentioned hydrogen bonds are clearly shown.

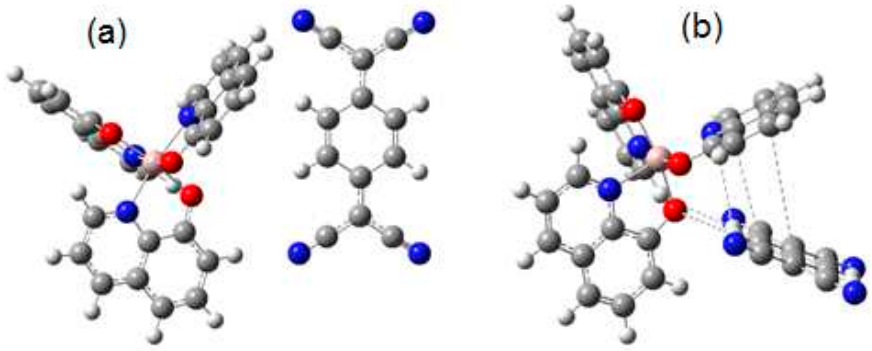

Figure 2. Optimized structures of (a) HAl-TCNQ1 and (b) HAl-TCNQ2.

Figure 3a,b shows the frontier molecular orbitals for HAl-TCNQ1, HOMO is located over hydroxyquinoline and LUMO over TCNQ, this result was expected because TCNQ is known for being an excellent electron acceptor [57]. The donor-acceptor behaviour of the species is the source of the interaction between them, the HOMO and LUMO values are 5.14 and 4.87 eV respectively, and the band gap value yields 0.271 eV. In order to measure the importance of the interaction between the molecules, Wiberg index were calculated. Table 1 shows the distance between the interacting atoms and the Wiberg index values. The calculations showed that three hydrogen bonds were formed between hydrogen atoms of hydroxyquinoline and TCNQ. In other hand Figure 3c,d shows the frontier molecular orbitals of HAl-TCNQ2, again HOMO is located over hydroxyquinoline and LUMO over TCNQ. In this case HOMO yields 5.44 eV and LUMO 4.47eV, whereas band gap value is 0.968 eV. Again, Wiberg index was calculated to analyse the interaction between atoms. In this case three hydrogen bridges were localized; Table 1 shows the distance and the Wiberg index for the involved atoms. It is observed that for the interaction O(51)-H(70) the Wiberg index is an order of magnitude higher and exhibits the smallest distance thus this is the main bond that leads the interaction. Based on the information, it is possible to conclude that both molecules constitute an electronic complex by means hydrogen bonds, its energy gap decreases and the semiconductor behavior is notably improved with the formation of this complexes. An explanation about this behavior can be that the intermolecular interaction (the hydrogen bond) directly arises from the HOMO of hydroxyquinoline and the LUMO of TCNQ which are localized in a very near energy values situation.

Preprints (www.preprints.org) | NOT PEER-REVIEWED | Posted: 13 July 2023 doi:10.20944/preprints202307.0905.v1

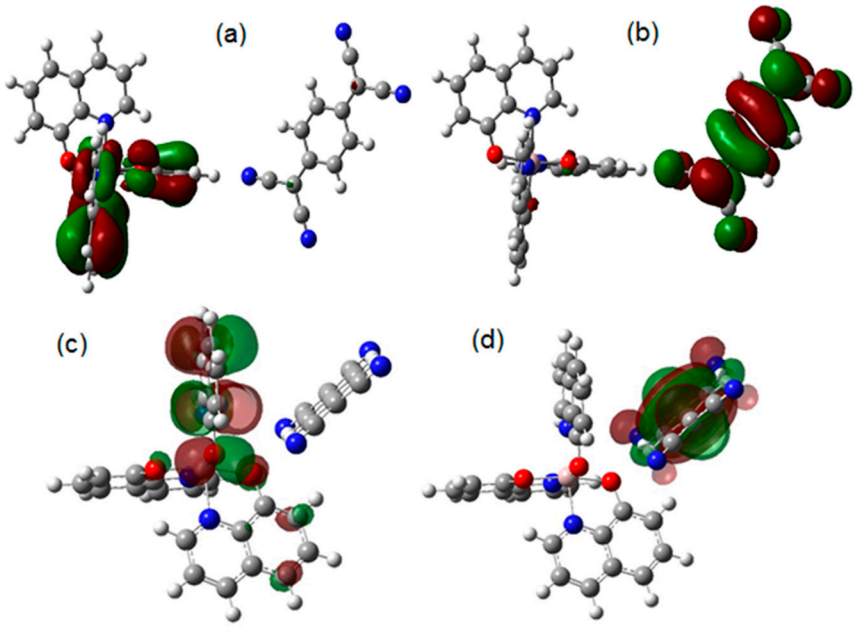

Figure 3. Frontier molecular orbitals for HAl-TCNQ1 (a) HOMO, (b) LUMO and HAl-TCNQ2 (c) HOMO, (d) LUMO.

It is important to consider that the values of 0.271 and 0.968 eV for HAl-TCNQ1 and HAl-TCNQ2 respectively, correspond to low band gap semiconductors [58,59]. Apparently, the donor-acceptor approach introduced by Havinga et al. [59] is the cause of the significant decrease in the band gap. The position of the HOMO and LUMO levels and the band gap of the resulting doped semiconductor are determined by an hybridization of the corresponding frontier orbitals of the Alq_3 and TCNQ units (see Figure 3). Therefore, according to the DFT calculations, it is convenient to carry out the experimental doping of Alq_3 with the TCNQ. Additionally, the IR spectra were theoretically obtained for both HAl-TCNQ1 and HAl-TCNQ2 (see Figure 4) and the results obtained by DFT calculations give hint of the feasibility to carry out the experimental doping of the semiconductor Alq_3-TCNQ.

Table 1. Distance and Wiberg index of the interacting atoms in HAl-TCNQ1 and HAl-TCNQ2.

	Distance (Å)			**Wiberg index**
Alq_3		**TCNQ**		**HAl-TCNQ1**
	N (62)	N (53)		
H (22)		2.85		0.0018
H (23)		2.76		0.0024
H (49)	2.49			0.0074
Alq_3		**TCNQ**		**HAl-TCNQ2**
	N (53)	H (69)	H (70)	
H (15)	2.69			0.0036
O (32)		3.04		0.0023
O (51)			2.079	0.0257

4.2. Fabrication and Characterization of Hybrid Film

After the doping, the Alq_3-TCNQ was characterized by IR spectroscopy in KBr pellet and these results was compared to the theoretically obtained; both spectra are shown in Figure 4. Characteristic peaks of Alq_3 bands at 400-650 cm^{-1} can be related to the stretching vibration of metal ion with attached ligand, while peak at 1582 cm^{-1} is associated to the quinoline group of Alq_3 [17,60–63],

Preprints (www.preprints.org) | NOT PEER-REVIEWED | Posted: 13 July 2023 doi:10.20944/preprints202307.0905.v1

additionally in the spectrum it is observed aromatic stretching C=C (1607 cm^{-1}). C-C (1469 cm^{-1}) and C-C-H bending vibrations (1169 cm^{-1}) are also present, while peaks at 781, 646 cm^{-1} is associated with in-plane ring deformations [17,60]. On the side of the TCNQ dopant the signal is observed at 2215 cm^{-1}, referring to the CN-stretching mode of the cyano groups [64]. To further understand the spectra, a more detailed analysis is presented in Table 2. The good agreement between the experimental IR spectrum and that theoretically obtained indicates that the calculations yield a good approach to the experimental study. Although apparently the HAl-TCNQ2 IR spectrum is more similar to the experimental spectrum. The changes presented in the experimental spectrum with respect to the theoretical spectra are due to the fact that in the spectra calculated by DFT, only the interaction between a hydroxyquinoline molecule and a TCNQ molecule is considered as isolated species, i.e. there are not other kind of interactions nor within similar molecules, nor with impurities, thus this spectra is very clean with respect its experimental counterpart. The multiple interactions between Alq_3 molecules and their dopant are reflected in the experimental spectrum; such interactions cause both bathochromic and hypsochromic shifts. Table 2 also presents the data for the IR spectrum of the (Alq_3-TCNQ):PPy film, which was carried out to verify that there was no degradation in the doped semiconductor after preparing the hybrid film, and the results show that there was no degradation.

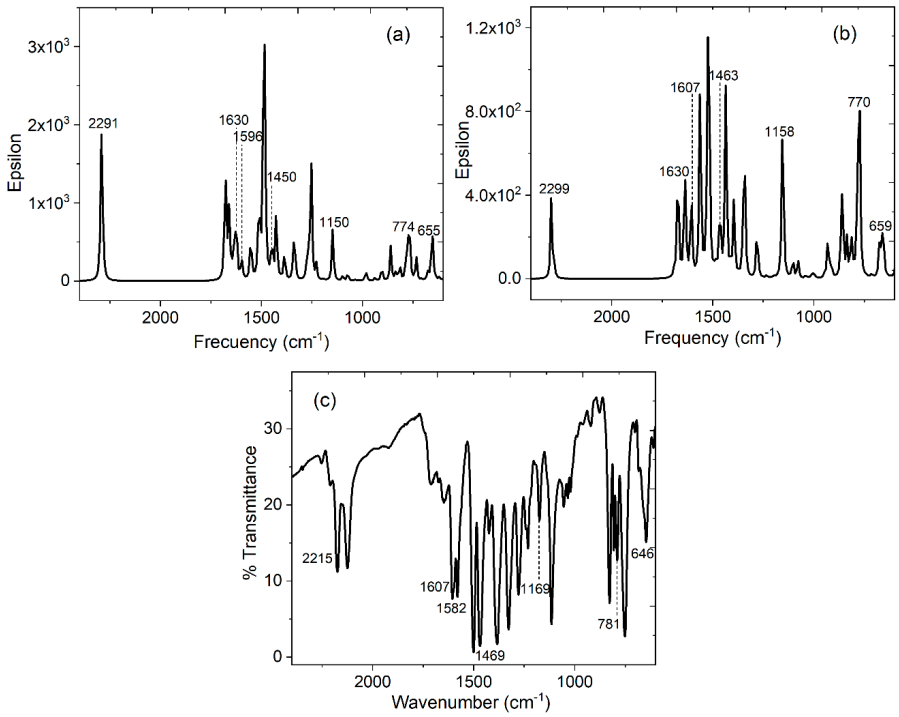

Figure 4. Calculated IR spectrum for (a) HAl-TCNQ1, (b) HAl-TCNQ2 and (c) experimental IR spectrum for Alq_3-TCNQ in KBr pellet.

Table 2. Calculated and experimental IR frequencies and their assignment for Alq_3-TCNQ.

HAl-TCNQ1 ν (cm^{-1}) simulated	HAl-TCNQ2 ν (cm^{-1}) simulated	Alq_3-TCNQ ν (cm^{-1}) KBr pellet	(Alq_3-TCNQ):PPy ν (cm^{-1}) film	Assignment
1630	1630	1607	1609	C=C
1596	1607	1582	1591	C=N
1450	1463	1469	1466	C-C
1150	1158	1169	1156	C-C-H
774, 655	770, 659	781, 646	772, 648	in-plane ring deformations
2291	2299	2215	2217	CN-stretchig mode

Preprints (www.preprints.org) | NOT PEER-REVIEWED | Posted: 13 July 2023 doi:10.20944/preprints202307.0905.v1

SEM was carried out in order to analyze the morphology of the (Alq_3-TCNQ):PPy film, and Figure 5a shows the 250x microphotography of the hybrid film. As can be seen, the film is made up of clusters of various sizes that are distributed along the entire surface. It is a heterogeneous film in terms of the shape and size of the clusters formed. To complement the information, the (Alq_3-TCNQ):PPy film was studied by MFA and as seen in Figure 5b, an irregular topography integrated by crests and valleys of different sizes is presented. This topography is reflected in a root mean square (RMS) of 23.04 nm and an arithmetic mean roughness (Ra) of 15.03 nm. Besides, considering a maximum applied force of 990 N, the mechanical properties of the hybrid film are (i) the unitary deformation (ε) = 0.744, (ii) the maximum stress (σ_{max}) = 8.66 MPa and (iii) the Knoop microhardness (HK) = 0.0311. For applications in organic optoelectronic devices, high mechanical resistance is required which, according to the results obtained, presents (Alq_3-TCNQ):PPy film.

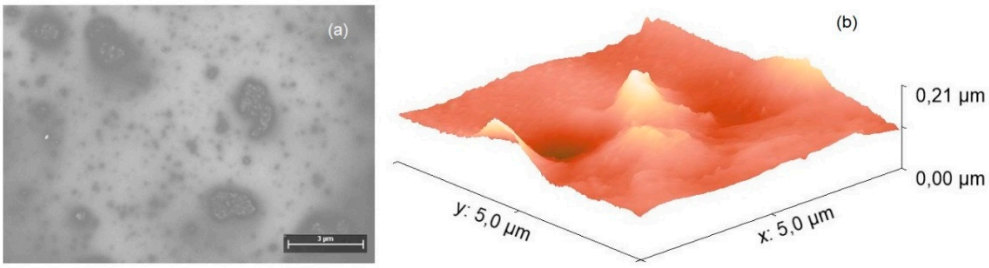

Figure 5. (a) SEM and (b) AFM measurements of (Alq_3-TCNQ):PPy film.

4.3. Optical Characterization of the device

Besides controlled band gap, active materials for electronic and photonic applications should present appropriate absorption and/or emission properties, highest occupied and lowest unoccupied molecular orbital energy levels and charge-transport properties. The UV-vis spectra of the semiconductor film are shown in Figure 6. If it is required to use the (Alq_3-TCNQ):PPy film in optoelectronic and photovoltaic devices, it is necessary to understand their optical behavior. In Figure 6a,b, the absorbance and transmittance respectively for the films are shown. In the absorbance spectrum of Alq_3-TCNQ film an absorption band in 375 nm is observed. It has been found that this energy absorption is due to the electron transition from the HOMO in the Alq_3 to the LUMO in the TCNQ [18]. In other context, there is also a small band at 860 nm, as a result of charge transfer with TCNQ. Regarding transmittance, the bands in the film becomes more noticeable and appears in the 570 to 800 regions. Another feature to notice in the spectrum of Figure 6b is the high transmittance at a larger wavelength of λ>900 nm; the transparency of around 80% at high wavelengths coincides with that obtained both for the Alq_3 precursor [20], and for other hydroxyquinolines such as zinc [18]. Apparently, even though it is doped and embedded in a polymeric matrix, hydroxyquinoline does not lose its transparency at high wavelengths.

Preprints (www.preprints.org) | NOT PEER-REVIEWED | Posted: 13 July 2023 doi:10.20944/preprints202307.0905.v1

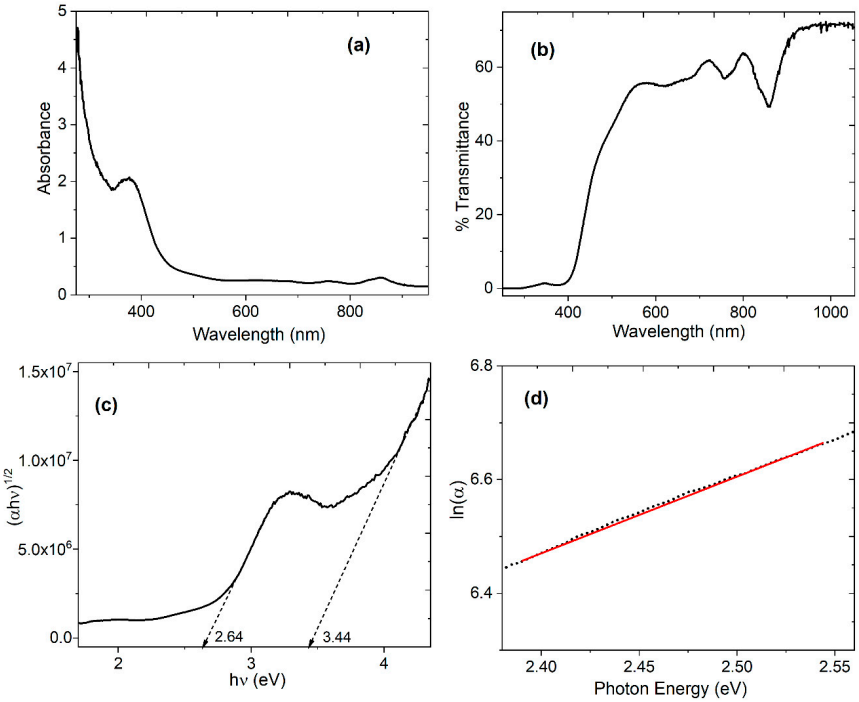

Figure 6. (a) Absorbance spectra, (b) % Transmittance, (c) Tauc plot and (d) variation of ln(α) with hν for (Alq_3-TCNQ):PPy film.

The optical band gap is the most relevant parameter to evaluate the potential of (Alq_3-TCNQ):PPy film for use in optoelectronic devices as active layers. The optical band gap (E_g^{opt}) was calculated through Tauc's semi-empirical model [65]. The calculation to obtain the optical bandgap with Tauc's method is based in the relation [66] $\alpha h\nu = B(h\nu - E_g^{opt})^n$, where h is Planck's constant, parameter B depends on the probability of transition, E_g^{opt} is the optical band gap and n is a number which characterizes the transition process, where n=2 for indirect allowed transitions. The absorption coefficient (α) and frequency (ν) are experimentally obtained from $\alpha = ln(T/d)$ and $\nu = \frac{c}{\lambda}$ respectively. In these expressions, T is the transmittance, d is the thickness of the film, c is the speed of light and λ is the wavelength. The dependence of $(\alpha h\nu)^n$ on $h\nu$ was plotted and E_g^{opt} was evaluated from the x-axis intercept at $(\alpha h\nu)^{1/2}$= 0. The values of E_g^{opt} calculated for the films are shown in Figure 6c. The (Alq_3-TCNQ):PPy shows two transitions; the first one at 2.64 eV is the onset gap (E_g^{onset}) and the second one at 3.44 eV corresponds to the optical gap (E_g^{opt}) [67]. This first transition corresponds to the optical absorption and formation of a bound electron-hole pair (Frenkel exciton) [66–68]. The second transition is the energy gap between the valence band, (π-band), and the conduction band, (π^*-band) [68]. The electronic transitions from π to π^* explain E_g^{onset} and E_g^{opt} as a consequence of several factors, including defects, film morphology, structural disorder and traps. However, the obtained value of 2.64 eV is less than the band gaps from 2.66 to 2.84 eV for pristine Alq_3 [18,20,23], it is also less than 3.97 eV for ZnO-doped Alq_3 [22] and also less than 3.2 eV for Alq_3 doped with sexithiophene [69]. The presence of TCNQ and PPy decrease the optical gap and also generates the onset gap, which is an indication of a more efficient semiconductor behavior in the (Alq_3-TCNQ):PPy film with respect to other semiconductors derived from Alq_3 like the ones mentioned above.

In other hand, the Urbach energy (E_U) can be used to determine the defects in the band gap and can be determined according to the equation [70,71]: $\alpha = A_a exp\left(\frac{h\nu}{E_U}\right)$, where in addition to the parameters defined above, A_a is a constant of the material that conforms to the α at the energy gap. The exponential absorption edge can be interpreted as due to the exponential distribution of local states in the energy band gap [70]. Figure 6d displays the linear relation between ln(α) and hν for the

Preprints (www.preprints.org) | NOT PEER-REVIEWED | Posted: 13 July 2023 doi:10.20944/preprints202307.0905.v1

hybrid films. The value of the E_U was determined from the reciprocal of the slope from this linear relation and in this case is 0.7594 eV. Assuming that E_U is zero in a perfect semiconductor, the value obtained is high, as a result of the bulk heterojunction between hydroxyquinoline, its dopant and the polymer. However; the interconnections between these three components of the hybrid film can generate charge transport both at the edges of Alq_3 and the TCNQ, and at the interface of the (Alq_3-TCNQ):PPy film with the electrodes, where charges are less common, and efficient when evaluating their electrical behavior. The number of satisfactorily dissociated charges depends on the magnitude of the internal field generated, and is limited by the charge mobility of each material.

4.4. Fabrication and Electrical Characterization of the device

In order to evaluate the electrical behavior in the (Alq_3-TCNQ):PPy film Figure 7 shows the I-V curves for the FTO/(Alq_3-TCNQ):PPy/Ag device under the different types of light used., It can be seen From Figure 7a that the behavior of the current is similar for all types of used light. In a visually fashion, an ohmic regime is appreciated from -1.2V to -1V, while the interval -1V to 0V shows another ohmic regime. A SCLC regime can be found from 0V to 0.6V and after 0.6V another ohmic regime is appreciated. Considering a cross-section area of 5.77mm^2 of the film, the current density-voltage (J-V) curves are shown in Figure 7b, where the same regimes can be seen in Figure 7a. Since the continuous functions that describe the current densities of the device are unknown, it is not possible to determine the exact values of voltage where the regime transitions occur, It has been applied the cubic-spline method [72] to each J-V curve to approximate a curve to the data from Figure 7b to fit cubic polynomials to the current densities data. From the cubic polynomials is easy to determine inflection points where there are changes in the concavity of the function and therefore in the current density. At some of these points, the ohmic to SCLC transition voltage V_{ON} and the trap-filled-limit voltage V_{TFL} are determined.

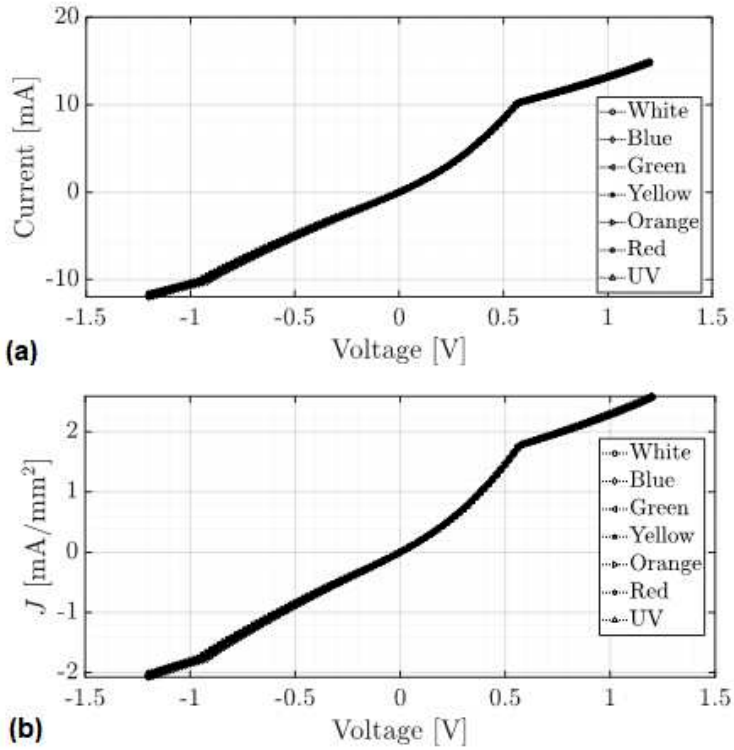

Figure 7. (a) Current-voltage curves and (b) current density-voltage curves of FTO/(Alq_3-TCNQ):PPy/Ag device.

The cubic polynomials are defined by $S_J(V) = J_i(V) = a_{3i}V^3 + a_{2i}V^2 + a_{1i}V + a_{0i}$ with $i = 0, \dots, k-1$. Notice that the spline function is defined as $S_J(V)\colon [a,b] \to \mathbb{R}$ where $a = V_0 \leq V_1 \leq \cdots \leq V_{k-1} \leq V_k = b$, and $V = (V_0, V_1, \dots, V_k)$ is the data vector, furthermore, each polynomial $J_i(V)$ is

Preprints (www.preprints.org) | NOT PEER-REVIEWED | Posted: 13 July 2023 doi:10.20944/preprints202307.0905.v1

defined as $J_i(V)$: $[V_i, V_{i+1}] \rightarrow \mathbb{R}$. Besides, a V_i^* point is an inflection point if $S_J'(V_i^*) = 0$ and $S_J''(V_i^*) > 0$. Applying the cubic-spline approach and the conditions for determining inflection points, 491 inflection points are obtained, the histogram of the voltage values where an inflection point is localized is shown in Figure 8.

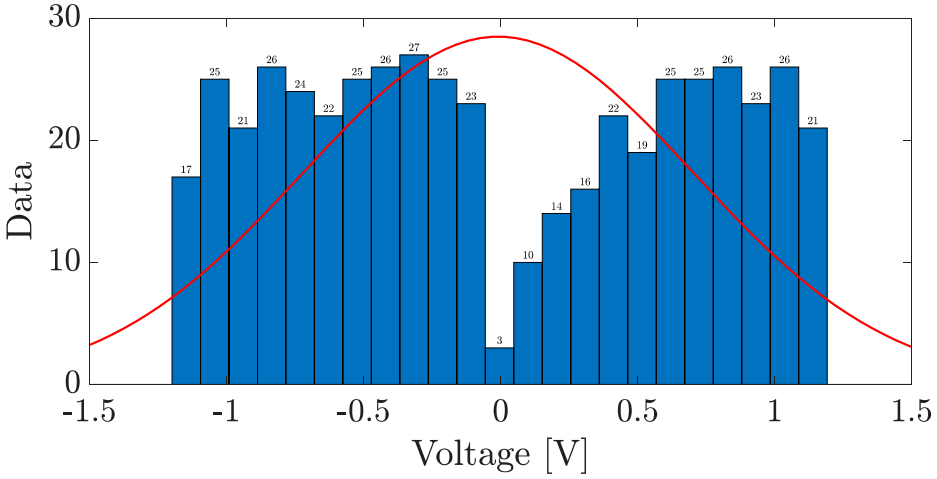

Figure 8. Inflection points histogram.

From Figure 8, the quartiles were set at 13, 56 and 70 percent of the data because at these data set the most significant concavity changes are presented. So, the voltage values where the most significant inflection points of the J-V curve exist are -0.88V, 0.16V and 0.54V. Therefore, the voltage intervals that define the different behaviors of the J-V curve are $I_1 \in [-1.2, -0.9]$, $I_2 \in [-0.9, 0.16]$ and $I_3 \in [0.16, 0.56]$. Based on these intervals, $V_{\text{ON}} = 0.16\,\text{V}$ and $V_{\text{TFL}} = 0.56\,\text{V}$. The approximation curves of the ohmic and SCLC regimes and the transition voltages are showed in Figure 9. From Figure 9, red curve represents the ohmic regime, which was approximated by a straight line, cyan curve is the quadratic SCLC regime, and it can be seen that V_{ON} joints these both regimes. On the other hand, V_{TFL} delimits the end of the quadratic SCLC regime. Since the regime after the V_{TFL} has an ohmic regime (magenta curve), it was also approximated by a straight line.

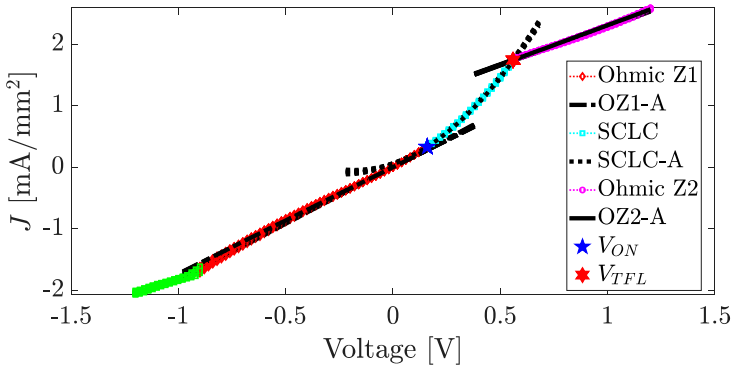

Figure 9. Approximation of the J-V graphs.

With the approximation of the ohmic to SCLC transition voltage V_{ON} and the trap-filled-limit voltage V_{TFL} and equations (3) and (4), the free carrier density n_0 and the trap density N_t can be determined as follows.

$$n_0 = \frac{9V_{ON}\varepsilon_0\varepsilon_r}{8qd_s^2} \tag{5}$$

$$N_t = \frac{2V_{TFL}\varepsilon_r}{qd_s^2} \tag{6}$$

Preprints (www.preprints.org) | NOT PEER-REVIEWED | Posted: 13 July 2023 doi:10.20944/preprints202307.0905.v1

Since $V_{ON} = 0.16$ V, $V_{TFL} = 0.56$ V, $q = 1.6 \times 10^{-19}$C, $\varepsilon_0 = 8.85418 \times 10^{-12} \frac{C}{Vm}$ $d_s = 1.14 \times 10^{-5}$m and assuming that the dielectric constant is $\varepsilon_r = 3.234$ which is dimensionless, an approximation of the free carrier density and trap density for the device are $n_0 = 2.4787 \times 10^{17} \frac{1}{m^3}$ and $N_t = 1.7419 \times 10^{29} \frac{1}{m^3}$ respectively.

5. Conclusions

In recent years, the optimization of the organic semiconductor manufacturing process has been a topic of scientific interest. In these optimization processes, new organic semiconductors are used, so it is necessary to have methodologies that allow to easily obtain the electrical characteristics of these materials, to determine if the device will have the best performance. In this sense, the hybrid film (Alq_3-TCNQ):PPy was fabricated by initially doping the hydroxyquinoline with the TCNQ and subsequently embedding the semiconductor in the polypyrrole polymer matrix. DFT calculations carried out on designed complexes of these species show that the nature of this complexes is ruled by the formation of hydrogen bonds which involve two possible cases (i) the interaction among nitrogen terminal atoms of TCNQ moiety with peripheral hydrogen atoms from the PPy and (ii) face to face interactions between TCNQ central hydrogen atoms and the heteroatoms from the organic rings of PPy. The formation of these complexes rules the decrease of the HOMO-LUMO gap as it shown by the same DFT calculations. The experimental IR spectra indicate that the hybrid film it did not suffer degradation during its deposit. The SEM and AFM images have confirmed that the film shows a heterogeneous morphology integrated by segregation of the Alq_3-TCNQ semiconductor in the matrix. The UV-vis spectrum of the (Alq_3-TCNQ):PPy film has showed a characteristic band at 375 nm attributed to the electro-transition from the HOMO orbital in hidroxiquinoline to the LUMO orbital in the TCNQ. The optical properties of the (Alq_3-TCNQ):PPy film showed two indirect allowed transitions with onset and optical gaps of 3.44 and 2.64 eV. Applying the cubic-spline method to the J-V curves of the device, it was determined that the ohmic to SCLC transition voltage is $V_{ON} = 0.16$V and the trap-filled-limit voltage is $V_{TFL} = 0.56$V, then considering that the dielectric constant is $\varepsilon_r = 3.234$, it was determined that the free carrier density and trap density for the device are $n_0 = 2.4787 \times 10^{17} \frac{1}{m^3}$ and $N_t = 1.7419 \times 10^{29} \frac{1}{m^3}$ respectively. Future work includes determination of the charge carrier mobility of the device. These results indicate that the (Alq_3-TCNQ):PPy film can be used as a component in OLED-type devices.

Author Contributions: Conceptualization, M.E.S.V. and R.S.; methodology, M.E.S.V., L.A.C.C., R.S., and C.R.; software, M.E.S.V., L.A.C.C. and R.S.; validation, M.E.S.V., L.A.C.C., R.S., and C.R.; formal analysis, M.E.S.V., C.R. and R.S.; investigation, L.A.C.C. and C.R.; resources, M.E.S.V., and R.S.; data curation, M.E.S.V., L.A.C.C., R.S., and C.R.; writing—original draft preparation, M.E.S.V., L.A.C.C., R.S., and C.R.; writing—review and editing, M.E.S.V., L.A.C.C., R.S. and C.R.; visualization, L.A.C.C. and C.R.; supervision, M.E.S.V. and R.S.; project administration, M.E.S.V.; funding acquisition, M.E.S.V. and R.S. All authors have read and agreed to the published version of the manuscript.

Funding: This research was funded by Anahuac México University, project number NNAIASEVM16070616. María Elena Sánchez Vergara gratefully acknowledges financial support from Consejo Mexiquense de Ciencia y Tecnología, Financiamiento para investigación de mujeres científicas: EDOMÉX-FICDTEM-2022-01, Project 64.

Institutional Review Board Statement: Not applicable.

Data Availability Statement: Data is contained within the article.

Acknowledgments: The authors are grateful for the technical support of Fernando Gibran Mendoza López, Valeria López Valenzuela and Jimena Sánchez. Also, we want to thank Cain González, María Teresa Vázquez, Celic Martínez, Alejandro Pompa and Oralia Jiménez for technical help.

Conflicts of Interest: The authors declare no conflict of interest.

References

1. Newman, C. R., Frisbie, C. D., da Silva Filho, D. A., Brédas, J.-L., Ewbank, P. C., & Mann, K. R. Introduction to organic thin film transistors and design of n-channel organic semiconductors. Chem. Mater. 2004, 16, 4436–4451. doi:10.1021/cm049391x
2. Dou, L., Liu, Y., Hong, Z., Li, G., & Yang, Y. Low-bandgap near-IR conjugated polymers/molecules for organic electronics. Chem. Rev. 2015, 115, 12633–12665. doi:10.1021/acs.chemrev.5b00165
3. Murphy, A. R., & Frechet, J. M. Organic semiconducting oligomers for use in thin film transistors. Chem. Rev. 2007, 107, 1066–1096. doi:10.1002/chin.200731215
4. Piradi, V., Yan, F., Zhu, X., & Wong, W.-Y. A recent overview of porphyrin-based π-extended small molecules as donors and acceptors for high-performance organic solar cells. Mater. Chem. Front. 2021, 5, 7119–7133. doi:10.1039/d1qm00952d
5. Henson, Z. B., Müllen, K., & Bazan, G. C. Design strategies for organic semiconductors beyond the molecular formula. Nat. Chem. 2012, 4, 699–704. doi:10.1038/nchem.1422
6. Sun, Y., Welch, G. C., Leong, W. L., Takacs, C. J., Bazan, G. C., & Heeger, A. J. Solution-processed small-molecule solar cells with 6.7% efficiency. Nat. Mater. 2012, 11, 44–48. https://doi.org/10.1038/nmat3160
7. Qin, Y., Li, G., Qi, T., & Huang, H. Aromatic imide/amide-based organic small-molecule emitters for organic light-emitting diodes. Mater. Chem. Front. 2020, 4, 1554–1568. doi:10.1039/d0qm00084a
8. Yu, T., Liu, L., Xie, Z., & Ma, Y. Progress in small-molecule luminescent materials for organic light-emitting diodes. Sci. China Chem. 2015, 58, 907–915. doi:10.1007/s11426-015-5409-7
9. Venkateswararao, A., & Wong, K.-T. Small molecules for vacuum-processed organic photovoltaics: past, current status, and prospect. Bull. Chem. Soc. Japan 2021, 94, 812–838. doi:10.1246/bcsj.20200330
10. Hains, A. W., Liang, Z., Woodhouse, M. A., & Gregg, B. A. Molecular semiconductors in organic photovoltaic cells. Chem. Rev. 2010, 110, 6689–6735. doi:10.1021/cr9002984
11. Yamao, T., Miki, T., Akagami, H., Nishimoto, Y., Ota, S., & Hotta, S. Direct formation of thin single crystals of organic semiconductors onto a substrate. Chem. Mater. 2007, 19, 3748–3753. doi:10.1021/cm071051z
12. Placencia, D., Wang, W., Shallcross, R. C., Nebesny, K. W., Brumbach, M., & Armstrong, N. R. Organic photovoltaic cells based on solvent-annealed, textured titanyl phthalocyanine/C60 heterojunctions. Adv. Funct. Mater. 2009, 19, 1913–1921. https://doi.org/10.1002/adfm.200801723
13. Gregg, B. A., Sprague, J., & Peterson, M. W. Long-range singlet energy transfer in perylene bis (phenethylimide) films. J. Phys. Chem. B 1997, 101, 5362–5369. doi:10.1021/jp9703263
14. Babu, B. H., Lyu, C., Yu, C., Wen, Z., Li, F., & Hao, X.-T. Role of Central Metal Ions in 8-Hydroxyquinoline-Doped ZnO Interfacial Layers for Improving the Performance of Polymer Solar Cells. Adv. Mater. Interfaces 2018, 5, 1801172. doi:10.1002/admi.201801172
15. Onlaor, K., Tunhoo, B., Thiwawong, T., & Nukeaw, J. Electrical bistability of tris-(8-hydroxyquinoline) aluminum (Alq3)/ZnSe organic-inorganic bistable device. Curr. Appl Phys. 2012, 12, 331–336. doi:10.1016/j.cap.2011.07.004
16. Shahedi, Z., Jafari, M. R., & Zolanvari, A. A. Synthesis of ZnQ_2, CaQ_2, and CdQ_2 for application in OLED: optical, thermal, and electrical characterizations. J. Mater. Sci. Mater. Electron. 2017, 28, 7313–7319. doi:10.1007/s10854-017-6417-5
17. Keshmiri, L., Elahi, S. M., Jafari, M. R., Jafari, F., & Parhizgar, S. S. The blue-shift of photoluminescence spectra of zinc complexes of 8-hydroxyquinoline by addition of ZnO nanoparticles. J. Electron. Mater. 2018, 47, 1526–1532. https://doi.org/10.1007/s11664-017-5956-0
18. Haggag, S. M., Farag, A. A., & Abdelrafea, M. Spectral, thermal and optical–electrical properties of the layer-by-layer deposited thin film of nano Zn(II)-8-hydroxy-5-nitrosoquinolate complex. Spectrochim. Acta A Mol. Biomol. Spectrosc. 2013, 110, 14–19. doi:10.1016/j.saa.2013.02.042
19. Painuly, D., Masram, D. T., Rabanal, M. E., & Nagpure, I. M. The effect of ethanol on structural, morphological and optical properties of Li(I) 8–hydroxyquinoline phosphor. J. Lumin. 2017, 192, 1180–1190. doi:10.1016/j.jlumin.2017.08.054
20. Sevgili, O., Canlı, S., Akman, F., Orak, I., Karabulut, A., & Yıldırım, N. Characterization of aluminum 8-hydroxyquinoline microbelts and microdots, and photodiode applications. J. Phys. Chem. Solids 2020, 136, 109128. doi:10.1016/j.jpcs.2019.109128
21. Demir, R., & Kaya, İ. Comparison of electrical characteristics of zinc oxide and cadmium sulfide films covered with 8-hydroxyquinoline for diode applications. J. Mater. Sci. Mater. Electron. 2019, 30, 7103–7109. doi:10.1007/s10854-019-01027-3
22. Babu, B. H., Lyu, C., Yu, C., Wen, Z., Li, F., & Hao, X.-T. Role of Central Metal Ions in 8-Hydroxyquinoline-Doped ZnO Interfacial Layers for Improving the Performance of Polymer Solar Cells. Adv. Mater. Interfaces 2018, 5, 1801172. doi:10.1002/admi.201801172
23. El-Nahass, M. M., Farid, A. M., & Atta, A. A. Structural and optical properties of Tris(8-hydroxyquinoline) aluminum (III)(Alq3) thermal evaporated thin films. J. Alloys Compd. 2010, 507, 112–119. doi:10.1016/j.jallcom.2010.07.110

24. Dai, C., Shang, F., Wei, Z., Chen, Z., Yan, X., Ji, Z., Pang, Z., Han, S. Room temperature ferromagnetic and optical properties of rare earth Sm-doped tris(8-hydroxyquinoline) gallium thin films. Thin Solid Films 2018, 648, 113–119. doi:10.1016/j.tsf.2018.01.001
25. Bakhshipour, S., Shahedi, Z., Mirahmadi, F., Fereidonnejad, R., & Hesani, M. Effect of different in situ temperatures on the crystallinity and optical properties of green synthesized 8-hydroxyquinoline zinc by saffron extract. Opt. Continuum 2022, 1, 1401–1412. doi:10.1364/optcon.459222
26. Dumur, F. Zinc complexes in OLEDs: An overview. Synth. Met. 2014, 195, 241–251. doi:10.1016/j.synthmet.2014.06.018
27. Shahedi, Z., Zare, H., & Sediqy, A. Manufacturing of nanoflowers crystal of ZnQ_2 by a co-precipitation process and their morphology-dependent luminescence properties. J. Mater. Sci. Mater. Electron 2021, 32, 6843–6854. doi:10.1007/s10854-021-05389-5
28. Requena, F., & Crespo, M. Recent advances on phosphorescent cycloplatinated compounds containing tetradentate nitrogen ligands for OLED applications. Inorg. Chem. Res. 2022, 6, 39–47. doi:10.22036/icr.2022.325512.1123
29. Jiang, F., Song, J., Dong, M., & Wang, Y. Preparation and Characterization of Paramagnetic Bis (8-Hydroxyquinoline) Manganese Crystals. Materials 2020, 13, 2379. doi:10.3390/ma13102379
30. Ghedini, M., La Deda, M., Aiello, I., & Grisolia, A. Synthesis and photophysical characterisation of soluble photoluminescent metal complexes with substituted 8-hydroxyquinolines. Synth. Met. 2003, 138, 189–192. doi:10.1016/s0379-6779(02)01261-4
31. Mohana, J., Ahila, G., Bharathi, M. D., & Anbalagan, G. Growth, spectral, optical, thermal, and mechanical behaviour of an organic single crystal: Quinolinium 2-carboxy 6-nitrophthalate monohydrate. J. Cryst. Growth 2016, 450, 181–189. doi:10.1016/j.jcrysgro.2016.06.044
32. Saeed, A., Razvi, M. A., & Salah, N. Third-order nonlinear optical properties of the small-molecular organic semiconductor tris (8-Hydroxyquinoline) aluminum by CW Z-scan technique. Results Phys. 2021, 24, 104162. doi:10.1016/j.rinp.2021.104162
33. Katakura, R., & Koide, Y. Configuration-specific synthesis of the facial and meridional isomers of tris(8-hydroxyquinolinate)aluminum (Alq3). Inorg. Chem. 2006, 45, 5730–5732. https://doi.org/10.1021/ic060594s
34. Rajeswaran, M., Blanton, T. N., Young, R. H., & Brennessel, W. Modeling Disorder in the Crystal Structure of the α Polymorph of Alq_3. J. Chem. Crystallogr.. 2010, 40, 195–200. https://doi.org/10.1007/s10870-009-9633-x
35. Kaji, H., Kusaka, Y., Onoyama, G., & Horii, F. Relationships between light-emitting properties and different isomers in polymorphs of tris(8-hydroxyquinoline) aluminum (III)(Alq3) analyzed by solid-state ^{27}Al NMR and density functional theory (DFT) calculations. Jpn. J. App. Phys. 2005, 44, 3706. doi:10.1143/JJAP.44.3706
36. Saeed, A., Al-Buriahi, M. S., Razvi, M. A., Salah, N., & Al-Hazmi, F. E. Electrical and dielectric properties of meridional and facial Alq_3 nanorods powders. J. Mater. Sci. Mater. Electron 2021, 32, 2075–2087. doi:10.1007/s10854-020-04974-4
37. McElvain, J., Antoniadis, H., Hueschen, M. R., Miller, J. N., Roitman, D. M., Sheats, J. R., & Moon, R. L. Formation and growth of black spots in organic light-emitting diodes. J. Appl. Phys. 1996, 80, 6002–6007. doi:10.1063/1.363598
38. Do, L.-M., Oyamada, M., Koike, A., Han, E.-M., Yamamoto, N., & Fujihira, M. Morphological change in the degradation of Al electrode surfaces of electroluminescent devices by fluorescence microscopy and AFM. Thin Solid Films 1996, 273, 209–213. doi:10.1016/0040-6090(95)06781-7
39. Tang, C. W., & VanSlyke, S. A. Organic electroluminescent diodes. Appl. Phys. Lett. 1987, 51, 913–915. doi:10.1007/978-3-642-93430-8_71
40. Lam, T.-N., Huang, Y.-L., Weng, K.-C., Lai, Y.-L., Lin, M.-W., Chu, Y.-H., Lin, H.-J., Kaun, C.-C, Wei, D.-H., Tseng, Y.-C, Hsu, Y.-J. Spin filtering of a termination-controlled LSMO/Alq_3 heterojunction for an organic spin valve. J. Mater. Chem. C 2017, 5, 9128–9137. https://doi.org/10.1039/C7TC02559A
41. Kao, P.-C., Chu, S.-Y., Huang, H.-H., Tseng, Z.-L., & Chen, Y.-C. Improved efficiency of organic photovoltaic cells using tris (8-hydroxy-quinoline) aluminum as a doping material. Thin Solid Films 2009, 517, 5301–5304. doi:10.1016/j.tsf.2009.03.147
42. Varo, P. L., Tejada, J. J., Villanueva, J. L., Carceller, J. E., & Deen, M. J. Modeling the transition from ohmic to space charge limited current in organic semiconductors. Org. Electron. 2012, 13, 1700–1709. doi:10.1016/j.orgel.2012.05.025
43. Abdel-Malik, T. G., & Cox, G. A. Charge transport in nickel phthalocyanine crystals. I. Ohmic and space-charge-limited currents in vacuum ambient. J. Phys. C: Solid State Phys. 1977, 10, 63. doi:10.1088/0022-3719/10/1/012
44. Moiz, S. A., Ahmed, M. M., & Karimov, K. S. Estimation of Electrical Parameters of OD Organic Semiconductor Diode from Measured I-V Characteristics. ETRI journal 2005, 27, 319–325. doi:10.4218/etrij.05.0104.0100

45. Kim, K. M., Choi, B. J., Lee, M. H., Kim, G. H., Song, S. J., Seok, J. Y., . . . Hwang, C. S. A detailed understanding of the electronic bipolar resistance switching behavior in Pt/TiO_2/Pt structure. Nanotechnology 2011, 22, 254010. doi:10.1088/0957-4484/22/25/254010
46. Kim, K. M., Choi, B. J., Shin, Y. C., Choi, S., & Hwang, C. S. Anode-interface localized filamentary mechanism in resistive switching of TiO_2 thin films. App. Phys. Lett. 2007, 91, 012907. doi:10.1063/1.2749846
47. Mott, N. F. & Gurney, R. W. Electronic processes in ionic crystals. Oxford, Second edition, 1946.
48. Gucciardi, P. G., Trusso, S., Vasi, C., Patane, S., & Allegrini, M. Nano-Raman imaging of Cu–TCNQ clusters in TCNQ thin films by scanning near-field optical microscopy. Phys. Chem. Chem. Phys. 2002, 4, 2747–2753. https://doi.org/10.1039/B110475F
49. Bendikov, M., Wudl, F., & Perepichka, D. F. Tetrathiafulvalenes, oligoacenenes, and their buckminsterfullerene derivatives: The brick and mortar of organic electronics. Chem. Rev. 2004, 104, 4891–4946. doi:10.1002/chin.200506263
50. Roncali, J. Molecular engineering of the band gap of π-conjugated systems: Facing technological applications. Macromol. Rapid Commun. 2007, 28, 1761–1775. doi:10.1002/marc.200700345
51. Frisch, M. J., Trucks, G. W., Schlegel, H. B., Scuseria, G. E., Robb, M., Cheeseman, J. R., Scalmani, G., Barone, V. P. G. A., Petersson, G. A., Nakatsuji, H. J. R. A. Gaussian 16, Revision A. 03, Gaussian. 2016 Inc., Wallingford CT, 3.
52. Becke, A. D. Density-functional exchange-energy approximation with correct asymptotic behavior. Phys. Rev. A 1988, 38, 3098. doi:10.1103/physreva.38.3098
53. Perdew, J. P., & Wang, Y. Accurate and simple analytic representation of the electron-gas correlation energy. Phys Rev. B 1992, 45, 13244. doi:10.1103/physrevb.45.13244
54. Min, D., Cho, M., Khan, A. R., & Li, S. Charge transport properties of dielectrics revealed by isothermal surface potential decay. IEEE Trans. Dielectr. Electr. Insul. 2012, 19, 1465–1473. doi:10.1109/tdei.2012.6260024
55. Varo, P. L., Tejada, J. J., Villanueva, J. L., & Deen, M. J. Space-charge and injection limited current in organic diodes: A unified model. Org. Electron. 2014, 15, 2526–2535. doi:10.1016/j.orgel.2014.05.039
56. Bhutta, M. S., Akram, S., Meng, P., Castellon, J., Agnel, S., Li, H., Guo, Y., Rasool, G., Hussain, S., Nazir, M.T. Steady-state conduction current performance for multilayer polyimide/SiO_2 films. Polymers 2021, 13, 640. doi:10.3390/polym13040640
57. Zhu, G.-Z., & Wang, L.-S. Communication: Vibrationally resolved photoelectron spectroscopy of the tetracyanoquinodimethane (TCNQ) anion and accurate determination of the electron affinity of TCNQ. J. Chem. Phys. 2015, 143, 221102. doi:10.1063/1.4937761
58. Scharber, M. C., & Sariciftci, N. S. Low band gap conjugated semiconducting polymers. Adv. Mater. Technol. 2021, 6, 2000857. doi:10.1002/admt.202000857
59. Havinga, E. E., Ten Hoeve, W., & Wynberg, H. J. A new class of small band gap organic polymer conductors. Polym. Bull. 1992, 29, 119–126. doi:10.1007/bf00558045
60. Phillips, J. P., & Deye, J. F. Infrared spectra of oxine chelates. Anal. Chim. Acta 1957, 17, 231–233. doi:10.1016/s0003-2670(00)87019-1
61. Gavrilko, T., Fedorovich, R., Dovbeshko, G., Marchenko, A., Naumovets, A., Nechytaylo, V., Puchkovska, G., Viduta, L., Baran, J., Ratajczak, H. FTIR spectroscopic and STM studies of vacuum deposited aluminium (III) 8-hydroxyquinoline thin films. J. Mol. Struct. 2004, 704, 163–168. doi:10.1016/j.molstruc.2004.01.068
62. Tackett, J. E., & Sawyer, D. T. Properties and infrared spectra in the potassium bromide region of 8-quinolinol and its metal chelates. Inorg. Chem. 1964, 3, 692–696. doi:10.1021/ic50015a021
63. Engelter, C., Jackson, G. E., Knight, C. L., & Thornton, D. A. Spectra-structure correlations from the infrared spectra of some transition metal complexes of 8-hydroxyquinoline. J. Mol. Struct. 1989, 213, 133–144. doi:10.1016/0022-2860(89)85112-9
64. Bredas, J. L., Silbey, R., Boudreaux, D. S., & Chance, R. R. Chain-length dependence of electronic and electrochemical properties of conjugated systems: polyacetylene, polyphenylene, polythiophene, and polypyrrole. J. Am. Chem. Soc. 1983, 105, 6555–6559. doi:10.1021/ja00360a004
65. Tauc, J. Optical properties and electronic structure of amorphous Ge and Si. Mater. Res. Bull. 1968, 3, 37–46. doi:10.1016/0025-5408(68)90023-8
66. Urbach, F. The long-wavelength edge of photographic sensitivity and of the electronic absorption of solids. Phys. Rev. 1953, 92, 1324. doi:10.1103/physrev.92.1324
67. Alosabi, A. Q., Al-Muntaser, A. A., El-Nahass, M. M., & Oraby, A. H. Structural, optical and DFT studies of disodium phthalocyanine thin films for optoelectronic devices applications. Opt. Laser Technol. 2022, 155, 108372. doi:10.1016/j.optlastec.2022.108372
68. Dongol, M., El-Nahass, M. M., El-Denglawey, A., Elhady, A. F., & Abuelwafa, A. A. Optical properties of nano 5, 10, 15, 20-tetraphenyl-21H,23H-prophyrin nickel (II) thin films. Curr. Appl Phys. 2012, 12, 1178–1184. doi:10.1016/j.cap.2012.02.051
69. Hill, I. G., Kahn, A., Soos, Z. G., & Pascal Jr, R. A. Charge-separation energy in films of π-conjugated organic molecules. Chem. Phys. Lett. 2000, 327, 181–188. doi:10.1016/s0009-2614(00)00882-4

70. Hamdalla, T., Darwish, A.A.A., Al-Ghamdi, S.A., Alzahrani, A.O.M., El-Zaidia, E.F.M., Alamrani, N.A., Elblbesy, M.A., Yahia, I. S. Preparation, Raman spectroscopy, surface morphology and optical properties of TiPcCl2 nanostructured films: thickness effect. Opt. Quantum. Electron. 2021, 53, 1–16. doi:10.21203/rs.3.rs-175277/v1
71. Ghanem, M. G., Badr, Y., Hameed, T. A., El Marssi, M., Lahmar, A., Wahab, H. A., & Battisha, I. K. Synthesis and characterization of undoped and Er-doped ZnO nano-structure thin films deposited by sol-gel spin coating technique. Mater. Res. Express 2019, 6, 085916. doi:10.1088/2053-1591/ab2750
72. De Boor, C. A practical guide to splines. Springer-verlag New York, 1978.